Improved Channel Occupancy Rate Estimation

Janne J. Lehtomäki, *Member, IEEE,* Miguel López-Benítez, *Member, IEEE,* Kenta Umebayashi, *Member, IEEE,* and Markku Juntti, *Senior Member, IEEE*

***Abstract*—Channel occupancy rate (COR) is the fraction of the time that a channel is occupied, i.e., contains signal(s) in addition to noise. Estimation of COR is important, e.g., in cognitive radio systems, which can use this information for intelligently adapting their spectrum use to the operating environment. For COR estimation, both the ability to operate with weak signals (sensitivity) and closeness of the estimate to the true COR value (accuracy) are important. In this paper, an improved COR estimation (iCOR) method is proposed enabling the use of high false alarm probabilities to improve sensitivity without the overestimation usually associated with high false alarm probabilities. The iCOR method is compared with the conventional method in terms of worst-case root-mean-square error (RMSE), which refers to the RMSE for the COR level yielding the maximum RMSE. To fairly compare different COR estimation methods, it is required that the RMSE for strong signals equals a target value and the considered methods are compared by their RMSE for weaker signals. Comprehensive theoretical analysis is performed and both exact results and approximations are derived. Experimental results verify the theoretical analysis and show significant sensitivity gains from the iCOR method (around 5 dB).**

***Keywords*—Channel occupancy rate, cognitive radio, duty cycle, energy detector, spectrum utilization, wireless LAN.**

I. Introduction

More efficient spectrum utilization and sharing are critically important for enabling wireless innovation and economic development [1]. For example, dynamic spectrum access (DSA) [2] using cognitive ratios (CRs) has been considered for more efficient spectrum utilization and for making more spectrum available. In the database approach the licensed (primary) users make entries in the database about their current and future spectrum utilization and the CRs can use this information along with their current location to find spectrum to use for their communication. The database approach is widely considered for the television (TV) bands [3]. However, in bands with more dynamic spectrum utilization the database based approach is less attractive and the spectrum sensing based approach has been widely studied. Therein the CRs use signal detection techniques to determine if other signals are present or not before making decision about their own transmissions [4]–[7].

Manuscript received August, 2014, revised December, 2014. This work was supported by the Research Council of the University of Oulu and by the Strategic Information and Communications R&D Promotion Programme (SCOPE).

J. Lehtomäki and M. Juntti are with the Centre for Wireless Communications (CWC), University of Oulu, Oulu, Finland.

M. López-Benítez is with the Department of Electrical Engineering and Electronics, University of Liverpool, United Kingdom.

K. Umebayashi is with the Graduate School of Engineering, Tokyo University of Agriculture and Technology, Tokyo, Japan.

Accurate spectrum sensing is often very challenging to realize [8]. However, it has been shown that spectrum sensing process can be significantly improved by using spectrum utilization information [9], which can also be used for adapting CRs' medium access control (MAC) parameters [10]. The 3GPP LTE (Long Term Evolution) Advanced small cells in unlicensed bands [11] could use the spectrum utilization information to find suitable component carrier center frequencies and bandwidths for use with the listen-before-talk technique while protecting co-existing users. Wireless local area networks such as WiFi over narrow channels (WiFi-NC) using multiple narrow channels could use the spectrum utilization information for channel selection in the 2.4 GHz industrial, scientific and medical (ISM) band, which has potentially a high level of fragmentation making channel selection difficult [12].

Spectrum utilization can be characterized, e.g., by duty cycle (DC) or channel occupancy rate (COR). Most spectrum utilization measurements are based on using a large number of frequency bins with each bin covering only a small bandwidth such as 100 kHz [13]. A radio frequency (RF) channel of a particular radio technology (or an arbitrary CR channel) usually consists of several frequency bins. The COR is the fraction of time that the considered channel is occupied, i.e., contains signal(s) in addition to noise only [14]–[16]. The COR is defined so that even if only a portion of the channel is occupied, the whole channel is considered as occupied [16]. The DC is a special case of the COR: the DC is the COR for a channel consisting of only a single frequency bin. Numerous spectrum utilization measurement campaigns have been performed focusing on measuring the DC in frequency bins [13], [17], [18]. Long-term measurement campaigns enable making accurate spectrum utilization models [13], [19], [20].

The COR can be estimated as the maximum DC value of frequency bins within the channel or by using an energy detector (ED) measuring the energy in the whole channel [16]. As mentioned in, e.g., [15], [16], [21] the ED can be implemented by summing up the measured powers for frequency bins within the considered channel. If the energy exceeds a threshold η, the channel is assumed to be occupied and otherwise it is assumed to be vacant. The calculation of the COR for arbitrary channels requires recording the measured power for each frequency bin in each frequency sweep. In [16], the MED-FCME CORϵ technique has been proposed for obtaining performance close to the ED but only requiring a binary value (1 or 0) to be stored for each frequency bin and sweep instead of a floating point value corresponding to the measured power. This leads to remarkably reduced storage requirements [22], which is important especially for long-term measurement campaigns.

The false alarm probability $P_{\rm fa}$ is the probability that the decision variable (such as energy) exceeds the threshold η when only noise is present. The value of η can be set based on the constant false alarm rate (CFAR) criterion so that $P_{\rm fa}$ equals a target value [5]. The statistics of the noise-only samples must be known to enable the threshold setting. Most works assume that the noise statistics are known. However, the knowledge of the signals to be detected is not required. In practice, the noise statistics can be determined, e.g., in a protected measurement space shielded from radio signals or while operating in a real environment. For example, we can measure a channel that is known to be idle (e.g., a TV channel that is known to be idle in the operating area of the CR device). Another option is to switch the RF front-end between the antenna and a matched load electronically so that the antenna is selected when transmitting/sensing and the matched load is selected when estimating/measuring the noise level of the channel. Even if no free channels are known, it is possible to estimate the noise level based on the received signal including both signals and noise [16], [23], [24]. These techniques could also be applied with the matched load, since very strong signals can leak to the receiver even with a matched load.

This manuscript considers estimation of COR. This is a problem different to spectrum sensing, which is performed in order to decide if a secondary user can begin transmitting or not. The performance metrics for spectrum sensing are detection probability (protection of primary users) and also false alarm probability (which reduces achieved rate of secondary communications). The performance for COR estimation is related to how close the estimated values are to the true ones. There are many metrics for estimators. We use root mean square error (RMSE) and the mean absolute error (MAE). False alarm probability in this work is not a performance metric but a design parameter, affecting estimation performance, that needs to be optimised for an accurate COR estimation.

With the conventional method, which counts the fraction of detections in a set of samples, high $P_{\rm fa}$ values such as 0.10 lead to severe overestimation, because the DC or the COR estimate is around 10%, even when no signals are present. Lower $P_{\rm fa}$ values result in less overestimation at the cost of much reduced sensitivity. In this paper, we propose an improved COR estimation (iCOR) method, which is able to suppress overestimation by using the knowledge of the value of $P_{\rm fa}$ to improve the tradeoff between the sensitivity and the estimation error. Our analysis focuses on the ED. However, the iCOR can be applied with any detection technique as long as $P_{\rm fa}$ can be set to an arbitrary target value. Our results are also applicable to DC estimation in addition to the COR estimation. Our contributions include the following:

1) We find closed-form expressions of the maximum allowed $P_{\rm fa}$ for a given estimation error level for the conventional method, which finds the COR estimate $\hat{\Psi}$ as the number of observations k exceeding the threshold divided by the total number of observations M, i.e., $\hat{\Psi} = k/M$, for the Bernoulli [14] and the m-out-of-M signal occupancy models.
2) We propose the iCOR method, which does not require any additional information compared to the conventional one. The iCOR output stays 0 until k is larger than a threshold depending on the used $P_{\rm fa}$ value. We find an approximation to the maximum allowed $P_{\rm fa}$ for the iCOR. The results show that the iCOR method is able to use a much higher $P_{\rm fa}$ than the conventional method while yielding the same RMSE levels of the COR estimates leading to significant sensitivity gains.
3) The derived theoretical expressions are validated by numerical examples and illustrations as well as real experiments with a spectrum analyzer.
4) We optimize the mapping function from k to the COR estimate $\hat{\Psi}$ using two different optimization criteria and compare the resulting performance with the performance of the iCOR method to confirm the good performance of the iCOR method.

The remainder of this paper is organized as follows. The performance equations for a single observation with the ED are presented in Section II. In Section III, we present models for signal occupancy which characterize signal presence in a sequence of M observations. In Section IV, we find the RMSE and MAE for a COR estimate with an arbitrary mapping function, derive truncated Gaussian approximation to the RMSE and MAE for an arbitrary clipped linear mapping function, and define the worst-case RMSE and the worst-case MAE. The specific analysis of the conventional COR estimation method is presented in Section V and the iCOR method is proposed and analyzed in Section VI. The measurement setup, and numerical and measurement results are presented in Section VII. In Section VIII, we compare the iCOR to two numerically optimized mapping functions to show its validity. Conclusions are presented in Section IX.

II. Signal Detection for Single Observation

Assume that N complex baseband temporal samples r_i, $i = 1, 2, \cdots, N$ are obtained during a single observation period. We follow the random signal model with complex sampling [7]

$$\begin{array}{ll} \mathcal{H}_0: & r_i = n_i \\ \mathcal{H}_1: & r_i = x_i + n_i \end{array} \tag{1}$$

where $\mathcal{H}_0$ refers to the hypothesis with only noise present and $\mathcal{H}_1$ denotes the case with also a signal present. Both noise and signal samples are assumed to be temporally and mutually independent, identically distributed (i.i.d) Gaussian. The noise samples (white due to the i.i.d assumption) $n_i \sim \mathcal{CN}\left(0, 2\sigma_{\rm n}^2\right)$ and the signal samples $x_i \sim \mathcal{CN}\left(0, 2\sigma_{\rm s}^2\right)$.

A. Conventional Energy Detection

The ED finds the sum of the magnitude-squared samples

$$V = \sum_{i=1}^{N} |r_i|^2. \tag{2}$$

1) Ideal ED: The probability of false alarm is [7]

$$P_{\rm fa} = \mathrm{Prob}\left(V > \eta | \mathcal{H}_0\right) = \tilde{\Gamma}\left(N, \frac{\eta}{2\sigma_{\rm n}^2}\right) \tag{3}$$

where $\tilde{\Gamma}$ is the regularized gamma function defined as $\tilde{\Gamma}(a,z)=\frac{1}{\Gamma(a)}\int_z^\infty t^{a-1}e^{-t}dt$ and $\Gamma(\cdot)$ is the gamma function [25, (6.1.1)]. Let us assume that the noise variance $\sigma_{\rm n}^2$ is perfectly known. Now, the threshold to obtain a given $P_{\rm fa}$ value is

$$\eta = 2\sigma_{\rm n}^2\tilde{\Gamma}^{-1}(N, P_{\rm fa}) \tag{4}$$

where $\tilde{\Gamma}^{-1}$ is the inverse of the regularized gamma function. The probability of detection, i.e., the probability of correctly detecting a signal present under $\mathcal{H}_1$, is [7][1]

$$P_{\rm d} = \text{Prob}\left(V>\eta|\,\mathcal{H}_1\right) = \tilde{\Gamma}\left(N, \frac{\tilde{\Gamma}^{-1}(N,P_{\rm fa})}{1+\text{SNR}}\right), \tag{5}$$

where the signal-to-noise ratio (SNR) is $\text{SNR}=\sigma_{\rm s}^2/\sigma_{\rm n}^2$.

2) ENP-ED: When using the energy detection with estimated noise power (ENP), the noise variance $\sigma_{\rm n}^2$ is estimated based on K reference samples [7], [26]. Following [7], the probability of detection for the random signal model for given $P_{\rm fa}$ and assuming noise-only reference samples (such as from a known free channel or from a matched load) is[2]

$$P_{\rm d} = I_x(K,N), \tag{6}$$

where $I_x(z,w)$ is the incomplete beta function defined as

$$I_x(z,w) = \frac{\Gamma(z+w)}{\Gamma(z)\Gamma(w)}\int_0^x t^{z-1}(1-t)^{w-1}dt, \tag{7}$$

where

$$x = \frac{1+\text{SNR}}{1/\zeta+\text{SNR}}, \tag{8}$$

and ζ is the solution of

$$P_{\rm fa} = I_\zeta(K,N). \tag{9}$$

B. FFT based Energy Detector

The fast Fourier transform (FFT) based ED divides the N samples into blocks of $N_{\rm FFT}$ samples. The time domain samples r_i for FFT block $l=1,2,\cdots,L$ are

$$\mathbf{r}_l = [r_i]_{i=(l-1)(1-\gamma)N_{\rm FFT}+1,\cdots,(l-1)(1-\gamma)N_{\rm FFT}+N_{\rm FFT}}, \tag{10}$$

where $\gamma\in[0,1]$ is the overlap ratio indicating the degree of overlapping between different FFT blocks ($\gamma N_{\rm FFT}$ is assumed to be an integer) and the number of blocks L is

$$L = \left\lfloor \frac{N-N_{\rm FFT}}{(1-\gamma)N_{\rm FFT}} \right\rfloor + 1, \tag{11}$$

where $\lfloor\ \rfloor$ denotes the floor function. A windowed FFT operation in each block can be represented as

$$\mathbf{y}_l = \mathbf{F}\mathbf{W}\mathbf{r}_l = [y_{0,l},\, y_{1,l},\cdots,\, y_{N_{\rm FFT}-1,l}]^T, \tag{12}$$

where $\mathbf{F}=\left(e^{-2\pi jki/N_{\rm FFT}}\right)_{j,k=0,1,\cdots,N_{\rm FFT}-1}$ is the discrete Fourier transform matrix, $\text{i}=\sqrt{-1}$, and the diagonal matrix $\mathbf{W}=\text{diag}\left(w_0,w_1,\cdots,w_{N_{\rm FFT}-1}\right)$ contains the real-valued window coefficients normalized as $\sum_{k=0}^{N_{\rm FFT}-1}w_k^2=1$. Different window functions have different pros and cons such as frequency resolution and spectral leakage [27]. The magnitude-squared frequency domain samples within the studied channel and from L FFT blocks are summed to find the decision variable V as [21]

$$V = \sum_{l=1}^{L}\sum_{i\in\Theta_s}|y_{i,l}|^2, \tag{13}$$

where Θ_s denotes the set of frequency bins within the studied channel s. The total number of magnitude-squared values used for finding V is $|\Theta_s|\,L$, where $|\cdot|$ denotes the cardinality of a set. The number of time-combined blocks L needs to be controlled to avoid overestimation resulting from the fact that with time-domain combining the output is not representing instantaneous channels state [16]. It is possible to control the overestimation by keeping N fixed so that the FFT size $N_{\rm FFT}$ is reduced as L is increased leading to reduced frequency resolution [24]. The frequency domain averaging over Θ_s does not lead to problems, since even if a part of the channel is occupied, it is classified as occupied [16]. The distribution of V under noise-only case $\mathcal{H}_0$ has been found in [21] for both $\gamma=0$ and $\gamma>0$. Because we did not use time-domain combining to avoid overestimation in the experimental tests there is no difference between these cases. Thus, we will use the results for $\gamma=0$ for an arbitrary L ($L=1$ corresponds to the experiments).

In order to determine the decision threshold for a particular $P_{\rm fa}$, let us define $|\Theta_s|\times|\Theta_s|$ matrix $\mathbf{A}$ [21]

$$[\mathbf{A}]_{pq} = \sum_{l=0}^{N_{\rm FFT}-1} w_l^2\exp\left(\frac{2\pi l(p-q)\,\text{i}}{N_{\rm FFT}}\right) \tag{14}$$

and let us denote the eigenvalues of matrix $\mathbf{A}$ as λ_i. Both exact results and approximations using these eigenvalues are presented in [21]. The exact results are numerically difficult to evaluate. Therefore, we use an accurate approximation found by using the results for weighted sums of chi-squared variables in [21], [28]:

$$\eta = \sigma_{\rm n}^2\left\{c_1 + 2\tilde{\Gamma}^{-1}\left(\frac{h'}{2}, P_{\rm fa}\right)\sqrt{\frac{c_2}{h'}} - \sqrt{c_2h'}\right\}, \tag{15}$$

where

$$c_j = 2L\sum_{i=1}^{N_{\rm FFT}}\lambda_i^j \tag{16}$$

and

$$h' = \frac{c_2^3}{c_3^2}. \tag{17}$$

The practical pulse waveforms used for communication are typically not random. However, the random data symbol pattern leads to frequency domain fluctuation [24], and we can approximate a signal as i.i.d Gaussian in frequency domain [16]. Since only the frequency bins within the considered channel are important, the SNR is defined as the average ratio

[1] `gammainc(gammaincinv(PFA,N,'upper')/(1+SNR),N,'upper')` in MATLAB

[2] `betainc((1+SNR)/(SNR+1/betaincinv(PFA,K,N)),K,N)`

between the signal and noise power within the considered channel (Θ_s). We get the probability of detection P_{d} for Gaussian signals in additive white Gaussian noise (AWGN) channel (corresponding to the random signal model) as

$$P_{\mathrm{d,AWGN}}\left(\mathrm{SNR}\right)=\tilde{\Gamma}\left(\frac{h'}{2},\frac{\alpha}{2}\sqrt{\frac{h'}{c_2}}\right) \tag{18}$$

where

$$\alpha=\frac{c_1+2\tilde{\Gamma}^{-1}\left(\frac{h'}{2},P_{\mathrm{fa}}\right)\sqrt{\frac{c_2}{h'}}-\sqrt{c_2h'}}{1+\mathrm{SNR}}-c_1. \tag{19}$$

If we also include the Rayleigh (flat) fading channel, we get

$$P_{\mathrm{d,RAYL}}\left(\mathrm{SNR}\right)=\int_0^\infty P_{\mathrm{d,AWGN}}\left(x\right)\frac{1}{\mathrm{SNR}}e^{-\frac{x}{\mathrm{SNR}}}dx, \tag{20}$$

where SNR refers now to the average signal-to-noise-ratio.

III. Signal Occupancy Model

We assume that the COR estimation is performed based on the results of M observations. Two models for signal occupancy are considered: 1) the Bernoulli model, and 2) the m-out-of-M model.

A. Bernoulli Model

The Bernoulli model corresponds to the case of binomial probability of success Ψ generating the signal occupancies. We want to estimate this fundamental parameter Ψ (the true COR level) based on a finite number of observations M [14]. Let us define p as the probability to observe the channel as occupied. Now,

$$p=\left(1-\Psi\right)P_{\mathrm{fa}}+\Psi P_{\mathrm{d}}, \tag{21}$$

where $P_{\mathrm{d}}<1$ leads to not all true signal occupancies being detected and $P_{\mathrm{fa}}>0$ leads to false alarms. Let us define p_k as the probability that k observations out of M are detected as occupied. We assume the independence between observations. It is reasonable for swept spectrum analyzers, since it takes time to visit a frequency again, but not valid for real-time spectrum analyzers, which sample the whole bandwidth simultaneously. Thus, p_k is given by the binomial probability mass function (PMF)

$$p_k=\left(\begin{array}{c}M\\k\end{array}\right)p^k(1-p)^{M-k}. \tag{22}$$

B. m-out-of-M Model

In the m-out-of-M model, the aim is to estimate the instantaneous COR $\Psi=m/M$, where m is the number of observations containing signals in the current observation period. In this model, we specify that a realization of an arbitrary process generating the occupancies led to m observations containing signals in the current observation period. By convolving the binomial PMFs corresponding to m observations with signals present ($\mathcal{H}_1$) and $M-m$ observations with only noise ($\mathcal{H}_0$),

$$p_k=\sum_{i=0}^{M-m}p_{k-i}^{\mathcal{H}_1}p_i^{\mathcal{H}_0} \tag{23}$$

where $k=0,1,\cdots,M$, and

$$p_z^{\mathcal{H}_0}=\left(\begin{array}{c}M-m\\z\end{array}\right)P_{\mathrm{fa}}^z(1-P_{\mathrm{fa}})^{M-m-z}, \tag{24}$$

$z=0,1,\cdots,M-m$ corresponding to the $M-m$ noise-only observations, and

$$p_z^{\mathcal{H}_1}=\left(\begin{array}{c}m\\z\end{array}\right)P_{\mathrm{d}}^z(1-P_{\mathrm{d}})^{m-z} \tag{25}$$

when $z=0,1,\cdots,m$ (and zero otherwise) corresponding to the m observations with signals.

IV. RMSE & MAE Analysis

The RMSE of the COR estimate is defined as

$$\mathrm{rmse}\left(\Psi\right)=\sqrt{\mathbb{E}\left[\left(\hat{\Psi}-\Psi\right)^2\right]}, \tag{26}$$

where $\mathbb{E}[\cdot]$ denotes expectation, Ψ is the true COR, and $\hat{\Psi}$ is the estimated COR. The MSE (square of RMSE) is equal to the sum of the variance of the estimator and its squared bias. For unbiased estimators, the RMSE is equal to the standard deviation. The MAE is defined as

$$\mathrm{mae}\left(\Psi\right)=\mathbb{E}\left[\left|\hat{\Psi}-\Psi\right|\right], \tag{27}$$

For example, if we say that a channel is actually busy for 80% of the time (the true COR) but we estimate it as busy for 75% of the time (estimated COR), both MAE and RMSE are 5%. In practice, the estimated COR is a random variable leading to differences between the metrics as the MAE puts less emphasis on large errors. We will consider both metrics with the main focus on the RMSE.

For any arbitrary function $\hat{\Psi}\left(k\right)$ mapping k to an COR estimate $\hat{\Psi}$, the RMSE is

$$\mathrm{rmse}\left(\Psi\right)=\sqrt{\sum_{k=0}^{M}\left[p_k\left(\hat{\Psi}\left(k\right)-\Psi\right)^2\right]}. \tag{28}$$

The corresponding MAE is

$$\mathrm{mae}\left(\Psi\right)=\sum_{k=0}^{M}p_k\left|\hat{\Psi}\left(k\right)-\Psi\right|. \tag{29}$$

A. Truncated Gaussian Approximation

Linear mapping functions are an important subset of the possible mapping functions. Let us assume a generic linear mapping function a_1k+a_0 where $a_1>0$. Since valid values

of $\hat{\Psi}$ are between 0 and 1, we use clipping leading to

$$\hat{\Psi}(k) = \begin{cases} 0 & a_1 k + a_0 < 0 \\ a_1 k + a_0 & 0 \le a_1 k + a_0 \le 1 \\ 1 & a_1 k + a_0 > 1 \end{cases} \tag{30}$$

Let us approximate the distribution of k with a normal distribution with mean μ_k and variance σ_k^2. For the Bernoulli model $\mu_k = Mp$ and $\sigma_k^2 = Mp(1-p)$. For the m-out-of-M model $\mu_k = mP_{\rm d} + (M-m)P_{\rm fa}$ and $\sigma_k^2 = mP_{\rm d}(1-P_{\rm d}) + (M-m)P_{\rm fa}(1-P_{\rm fa})$. The clipping in $\hat{\Psi}$ can be represented by limiting the values of k. Let us denote the limited values of k as k'. The values of $k > (1-a_0)/a_1$ are set to $k' = b = (1-a_0)/a_1$ so that $a_1 b + a_0 = 1$ and the values of $k < -a_0/a_1$ are set to $k' = a = -a_0/a_1$ so that $a_1 a + a_0 = 0$.

Let us define $\mu_{k',1} = \mathbb{E}[k']$ and $\mu_{k',2} = \mathbb{E}\left[k'^2\right]$. We find $\mu_{k',1}$ by using the theory of truncated Gaussian variables [29] and by taking into account the clipping leading to

$$\mu_{k',1} = a d_4 + \mu_k (d_3 - d_4) - b(d_3 - 1) - \sigma_k (d_1 - d_2), \tag{31}$$

where

$$\begin{aligned} d_1 &= \phi\left((b-\mu_k)/\sigma_k\right), \\ d_2 &= \phi\left((a-\mu_k)/\sigma_k\right), \\ d_3 &= \Phi\left((b-\mu_k)/\sigma_k\right), \\ d_4 &= \Phi\left((a-\mu_k)/\sigma_k\right), \end{aligned} \tag{32}$$

and ϕ and Φ denote the density and cumulative distribution functions of the standard normal random variable, respectively. Similarly, we get $\mu_{k',2}$ as

$$\begin{aligned} \mu_{k',2} = &\left(\sigma_k^2 \left(\frac{\frac{d_2(a-\mu_k)}{\sigma_k} - \frac{d_1(b-\mu_k)}{\sigma_k}}{d_3 - d_4} - \frac{(d_1-d_2)^2}{d_3^2} + 1 \right) \right. \\ &\left. + \left(\mu_k - \frac{\sigma_k(d_1-d_2)}{d_3-d_4}\right)^2 \right) \\ &\times (d_3 - d_4) + a^2 d_4 - b^2 (d_3 - 1) \end{aligned} \tag{33}$$

Finally, we get an approximation to the RMSE for any linear mapping function as

$$\begin{aligned} \mathrm{rmse}(\Psi) &\approx \sqrt{\mathbb{E}\left[(a_1 k' + a_0 - \Psi)^2\right]} \\ &= \sqrt{\mathbb{E}\left[a_1^2 k'^2 + 2a_1(a_0 - \Psi)k' + (a_0 - \Psi)^2\right]} \\ &= \sqrt{a_1^2 \mu_{k',2} + 2a_1(a_0 - \Psi)\mu_{k',1} + (a_0 - \Psi)^2}. \end{aligned} \tag{34}$$

In order to find an approximation to the MAE, we define $\vartheta_1 = \mathbb{E}[(a_1 k' + a_0 - \Psi)] = a_1 \mu_{k',1} + a_0 - \Psi$ and $\vartheta_2^2 = \rho - \vartheta_1^2$, where $\rho = \mathbb{E}\left[(a_1 k' + a_0 - \Psi)^2\right]$, which is equal to the square of (34). The parameters ϑ_1 and ϑ_2^2 correspond to the mean and variance of $a_1 k' + a_0 - \Psi$, respectively. Since the absolute value of a normal random variable follows the folded normal distribution [30], we get

$$\begin{aligned} \mathrm{mae}(\Psi) &\approx \mathbb{E}[|a_1 k' + a_0 - \Psi|] \\ &= \vartheta_2 \sqrt{2/\pi} \exp\left(-\vartheta_1^2/2\vartheta_2^2\right) + \vartheta_1 \left[1 - 2\Phi\left(-\vartheta_1/\vartheta_2\right)\right]. \end{aligned} \tag{35}$$

B. Worst-case RMSE & MAE

Since Ψ is unknown, it is reasonable to consider the worst-case RMSE of a COR estimator, i.e.,

$$\mathrm{rmse}_{\max} = \max_{\Psi \in [0,1]} \mathrm{rmse}(\Psi). \tag{36}$$

to characterize estimation error. As the worst-case RMSE is found by considering all possible Ψ values, it includes RMSE with only noise present ($\Psi = 0$). **In the remainder of this paper, we require that the worst-case RMSE of the considered COR estimators when $P_{\rm d} = 1$ is less than or equal to $\lambda_{\rm W,RMSE}$.** The specified constraint value $\lambda_{\rm W,RMSE}$ (such as 0.05) determines the maximum allowed $P_{\rm fa}$. The constraint value is defined for $P_{\rm d} = 1$. Guaranteed worst-case RMSE with strong signals, i.e., $P_{\rm d} \approx 1$, is reasonable, since at least with strong easy-to-detect signals the COR estimators should give a good performance. Performance of different estimators is then compared by their RMSE with medium to low signal powers, i.e., $P_{\rm d} < 1$.

Similarly, the worst-case MAE is

$$\mathrm{mae}_{\max} = \max_{\Psi \in [0,1]} \mathrm{mae}(\Psi) \tag{37}$$

and the constraint value in terms of MAE for $P_{\rm d} = 1$ is denoted as $\lambda_{\rm W,MAE}$.

V. Conventional COR Estimator

The conventional DC/COR estimate is [13], [14], [18]

$$\hat{\Psi} = \frac{k}{M} \tag{38}$$

corresponding to $a_1 = 1/M$ and $a_0 = 0$, and k is the number of observations out of M total samples whose decision variables exceed the threshold η.

A. Bernoulli Model

The RMSE for the Bernoulli model is

$$\begin{aligned} \mathrm{rmse}(\Psi) &= \sqrt{\mathbb{E}\left[\left(\tfrac{k}{M} - \Psi\right)^2\right]} \\ &= \sqrt{\mathbb{E}\left[\left(\tfrac{k}{M}\right)^2\right] - 2\Psi\mathbb{E}\left[\tfrac{k}{M}\right] + \Psi^2} \\ &= \sqrt{\tfrac{p(1-p)}{M} + p^2 - 2\Psi p + \Psi^2}, \end{aligned} \tag{39}$$

where p is given in (21) and the expected values are obtained from the properties of the binomial random variables. We get the maximum allowed $P_{\rm fa}$ for the Bernoulli model for given constraint $\lambda_{\rm W,RMSE}$ as (42) on p. 7 (the proof is in Appendix A). We point out that

$$\lim_{M \to \infty} P_{\rm fa}^* = \lambda_{\rm W,RMSE} \tag{40}$$

Typically, $\Psi = 0$ (or close to 0) is the the worst-case. When $\Psi = 0$, the error is solely from the false alarms leading to $\mathrm{RMSE} \approx P_{\rm fa}$. One might think that by subtracting $P_{\rm fa}$ from the estimated COR, i.e.,

$$\hat{\Psi} = \frac{k}{M} - P_{\rm fa} \tag{41}$$

we could remove the bias of the estimate due to false alarms. However, it would just move the worst-case RMSE to occur at $\Psi = 1$ instead of (say) $\Psi = 0$. The reason is that when $\Psi = 1$ and $P_{\rm d} = 1$, all observations are detected leading to $k = M$ so that $\hat{\Psi} = 1 - P_{\rm fa}$. Since the real value $\Psi = 1$, this corresponds to $\mathrm{RMSE} = P_{\rm fa}$ leading to no improvement.

B. m-out-of-M Model

We use (28) together with (23) and obtain the optimization problem for finding the maximum allowed $P_{\rm fa}$ (to achieve good sensitivity):

$$\begin{aligned} \max \quad & P_{\rm fa} \\ \text{s.t.} \quad & \max_{m\in\{0,1,\cdots,M\}} \sqrt{\sum_{k=0}^{M}\left[p_k(k-m)^2\right]} \le M\lambda_{\rm W,RMSE}, \\ & 0 \le P_{\rm fa} \le 1,\ P_{\rm d} = 1 \end{aligned} \tag{43}$$

where p_k depends on $P_{\rm fa}$ as shown in (23). Since

$$\begin{aligned} &\sum_{k=0}^{M} p_k(k-m)^2 = (M-m)\,P_{\rm fa}\,(1-P_{\rm fa}) + (M-m)^2 P_{\rm fa}^2 \\ &= \left[(M-m)\,P_{\rm fa} + \tfrac{(1-P_{\rm fa})}{2}\right]^2 - \tfrac{(1-P_{\rm fa})^2}{4} \end{aligned} \tag{44}$$

reaches its maximum when $m = 0$ we use $m = 0$ to get the maximum allowed $P_{\rm fa}$ as

$$P_{\rm fa}^{*} = \frac{\sqrt{4\left(M^2 - M\right)\lambda_{\rm W,RMSE}^2 + 1} - 1}{2\left(M-1\right)} \tag{45}$$

when $0 \le \lambda_{\rm W,RMSE} \le 1$ and otherwise there is no solution. The above solution is exactly the same as that for the Bernoulli model when $\Psi = 0$ is its worst-case. This is reasonable, since, when $\Psi = 0$, there is no difference between the Bernoulli and m-out-of-M models.

VI. Improved COR Estimator

A. Bernoulli Model

Because the SNR, and thus $P_{\rm d}$, are assumed to be unknown, we find the maximum likelihood estimator (MLE) of Ψ for $P_{\rm d} = 1$. Because the constraint $\lambda_{\rm W,RMSE}$ is specified for $P_{\rm d} = 1$, this makes $P_{\rm d} = 1$ a reasonable choice, but does not mean that during the actual operation $P_{\rm d}$ should be very close 1, although high $P_{\rm fa}$ values enabled by the iCOR do increase $P_{\rm d}$. The choice $P_{\rm d} = 1$ is just an assumption used to derived the MLE which is then used for the actual input signal with unknown $P_{\rm d}$. In the numerical and experimental results in Section VII, we present performance as a function of SNR leading to varying $P_{\rm d}$ (from almost 0 to almost 1).

The MLE for (22) assuming $P_{\rm d} = 1$ is

$$\begin{aligned} \hat{\Psi}\left(k\right) = \max_{\tilde{\Psi}\in[0,\,1]} \Bigg\{ &\binom{M}{k} \left[\left(1-\tilde{\Psi}\right)P_{\rm fa} + \tilde{\Psi}\right]^k \\ &\times \left[1 - \left(1-\tilde{\Psi}\right)P_{\rm fa} - \tilde{\Psi}\right]^{M-k} \Bigg\} \end{aligned} \tag{46}$$

and by taking the derivative of the expression inside the curly brackets with respect to $\tilde{\Psi}$ and setting the result equal to zero we obtain

$$\hat{\Psi}\left(k\right) = \frac{\frac{k}{M} - P_{\rm fa}}{1 - P_{\rm fa}}. \tag{47}$$

If $\hat{\Psi}$ is negative, it is not a valid outcome and the boundary point zero is selected instead, i.e.,

$$\hat{\Psi}\left(k\right) = \begin{cases} \frac{\frac{k}{M} - P_{\rm fa}}{1 - P_{\rm fa}} & k \ge MP_{\rm fa} \\ 0 & k < MP_{\rm fa} \end{cases} \tag{48}$$

We refer to this approach as the iCOR method. The exact RMSE for iCOR can be obtained with (28) and the coefficients for the truncated Gaussian approximation are

$$a_1 = -\frac{1}{M\left(P_{\rm fa} - 1\right)}, \tag{49}$$

$$a_0 = \frac{P_{\rm fa}}{P_{\rm fa} - 1}. \tag{50}$$

Even with the truncated Gaussian approximation it is difficult to find the maximum allowed $P_{\rm fa}$ for given $\lambda_{\rm W,RMSE}$. Therefore, we use the standard (untruncated) Gaussian approximation. Straightforwardly, we obtain an approximation

$$P_{\rm fa}^{*} \approx 1 - \frac{1}{M\lambda_{\rm W,RMSE}^2 + 1}, \tag{51}$$

which is reasonably accurate when $M \ge 1000$ and $0.02 \le \lambda_{\rm W,RMSE} \le 0.09$. In Section VII-B, we use the exact $P_{\rm fa}$ values found with a numerical search but also state the values obtained with the above approximation.

B. m-out-M Model

The MLE for $P_{\rm d} = 1$ and the m-out-of-M model is

$$\hat{\Psi}\left(k\right) = \frac{1}{M} \max_{m\in\{0,1,\cdots,k\}} \binom{M-m}{k-m} P_{\rm fa}^{k-m}(1-P_{\rm fa})^{M-k} \tag{52}$$

which can be found by a numerical search over a finite set. Since the resulting mapping function is very close to the iCOR, we will apply the iCOR also for the m-out-of-M model.

VII. Numerical and Experimental Results

In this section, we present the measurement setup (VII-A) used in the experimental tests. Then in sections VII-B–VII-C we present both exact theoretical results and the results with the truncated Gaussian approximation. Finally, we show both measurements results and theoretical results in section VII-D.

A. Measurement Methodology

The measurement setup is summarized in Table I. The studied band is the 2400–2500 MHz ISM band which the instrument covers by using five FFT frequency segments each covering 20 MHz. The time required to collect the samples for one FFT segment was around 10 μs. To avoid overestimation we did not apply time-domain combining, i.e.,

$$P_{\mathrm{fa}}^{*} = \begin{cases} \frac{2\,M\,\lambda_{\mathrm{W,RMSE}}\sqrt{4\,M\,\lambda_{\mathrm{W,RMSE}}^{2}-1}-4\,M\,\lambda_{\mathrm{W,RMSE}}^{2}+1}{(4\,M^{2}-4M)\lambda_{\mathrm{W,RMSE}}^{2}+1} & \sqrt{\frac{1}{4M}} \le \lambda_{\mathrm{W,RMSE}} \le \sqrt{\frac{\sqrt{8M+1}-4M+1}{8M-8M^{2}}} \\ \frac{-\frac{1}{M}+\sqrt{4\lambda_{\mathrm{W,RMSE}}^{2}(1-1/M)+1/M^{2}}}{2(1-1/M)} & 1 \ge \lambda_{\mathrm{W,RMSE}} > \sqrt{\frac{\sqrt{8M+1}-4M+1}{8M-8M^{2}}} \\ \text{No solution possible} & \text{otherwise} \end{cases} \tag{42}$$

where $\sqrt{\frac{1}{4M}}$ is the ultimate performance limit with the Bernoulli model and 1 is the maximum possible RMSE.

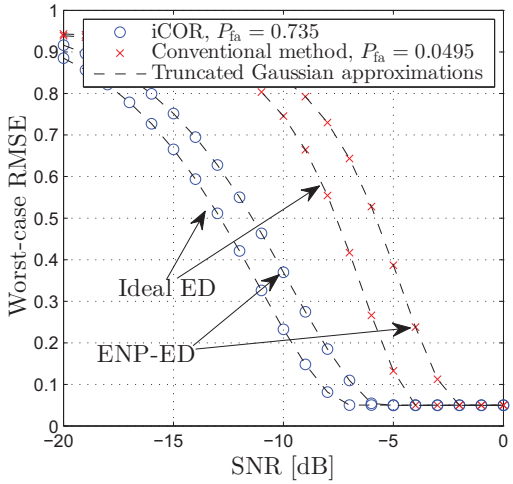

Fig. 1. Worst-case RMSE, $M = 1000$, ideal ED with $N = 100$, ENP-ED with $N = 100$ and $K = 100$, $\lambda_{\mathrm{W,RMSE}} = 0.05$, Bernoulli model.

$L = 1$. Signal following the IEEE 802.11b standard is generated with a signal generator with a random payload. The reference COR $\Psi = 0.40$ is obtained by controlling the idle time between packets. The signal generator output is connected to a channel emulator input and the channel emulator output is connected to the measurement system input. With this approach measurements can be controlled with a high precision. Both AWGN and time-variant and frequency selective ETSI BRAN WLAN model A (corresponding to a typical office environment) channels are utilized. We measured 100 000 noise-only ED decision variables in a measurement chamber shielded from radio signals (matched load was used to further suppress any possible signals) to estimate σ_{n}^{2} and to set threshold for any target P_{fa} with (15).

B. iCOR vs Conventional Method

Figs. 1 and 2 show the worst-case RMSE for iCOR and conventional COR estimation methods for $M = 1000$ observations and the ED (both ideal and ENP-ED with $K = 100$) with $N = 100$ complex samples used for each observation. Results show an excellent agreement of the truncated Gaussian approximation to the exact theoretical results by (28). Since M is large, the used occupancy model is not significantly affecting the results. The noise estimation in the ENP-ED results in a few dB loss.

The gain of the proposed iCOR method for $\lambda_{\mathrm{W,RMSE}} = 0.05$ (Fig. 1) is around 4 dB at the worst-case RMSE $= 0.1$, and around 7 dB at RMSE $= 0.8$. For $\lambda_{\mathrm{W,RMSE}} = 0.02$ in Fig. 2 the iCOR gain is around 2 dB at RMSE $= 0.1$, and around 4 dB at RMSE $= 0.8$. Therefore, the improvement observed is around 4–7 dB in Fig. 1 and 2–4 dB in Fig. 2.

The performance advantage of the iCOR estimator stems from the fact that it allows using a much higher P_{fa} value for the same RMSE constraint level $\lambda_{\mathrm{W,RMSE}}$ as compared to the conventional COR estimation method. For $\lambda_{\mathrm{W,RMSE}} = 0.05$, the conventional method can use $P_{\mathrm{fa}} = 0.0495$ while iCOR can use $P_{\mathrm{fa}} = 0.735$ (approximation (51) gives 0.71). For

TABLE I. MEASUREMENT SETUP

Instrument	Agilent N6841A
Center frequency	2450 MHz
Frequency span	100 MHz
Resolution bandwidth	242.27 kHz
Frequency bin separation	109.375 kHz
Window type	Gausstop window
N_{FFT} (in a frequency segment)	256
L	1
Digital IF bandwidth	20 MHz
Number of frequency points	916
Sweep time	≈10 ms
Filter	Creowave filter
Band-pass frequency range	2400–2500 MHz
Insertion loss (pass-band)	0.8 dB
Rejection bands	0–2300 MHz & 2600–5500 MHz
Rejection at rejection bands	≥90 dB
Low noise amplifier	Mini-Circuits ZRL-3500
Frequency range	700–3500 MHz
Gain (2.45 GHz)	19.5 dB
Noise Figure (2.45 GHz)	2.5 dB
Signal generator	Agilent E4438C ESG
Signal type	IEEE 802.11b
Actual COR level Ψ	0.40
Data rate	11 Mbit/sec
Total packet size	1508 bytes
Center frequency	2472 MHz
Channel emulator	EB Propsim F8
Channel types	AWGN ETSI WLAN A
Channel for COR estimation	IEEE 802.15.4 channel
Number of frequency bins $\lvert\Theta_s\rvert$	18
Bandwidth	2 MHz
Offset to the signal center freq.	7 MHz

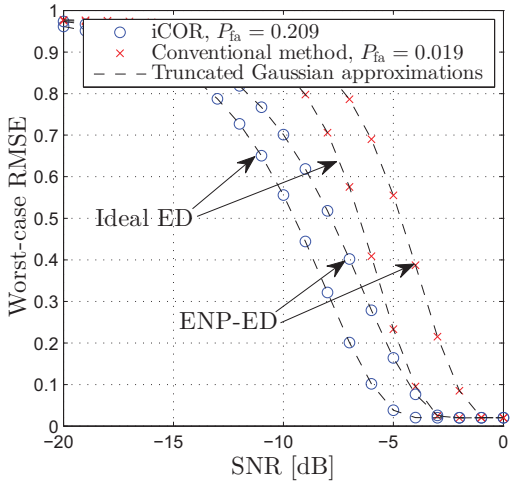

Fig. 2. Worst-case RMSE, $M = 1000$, ideal ED with $N = 100$, ENP-ED with $N = 100$ and $K = 100$, $\lambda_{\rm W,RMSE} = 0.02$, Bernoulli model.

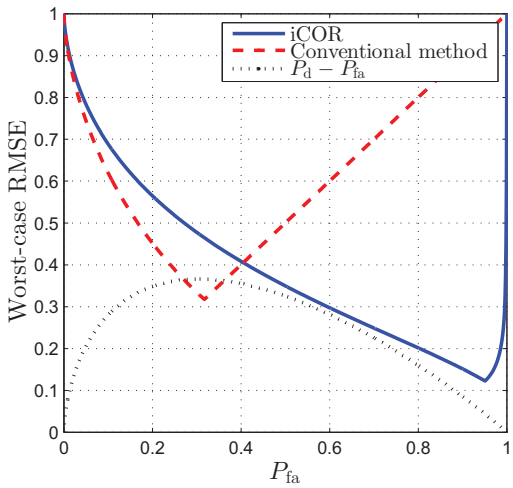

Fig. 3. Worst-case RMSE as a function of $P_{\rm fa}$, SNR $= -10$ dB, $M = 1000$, ideal ED with $N = 100$, Bernoulli model.

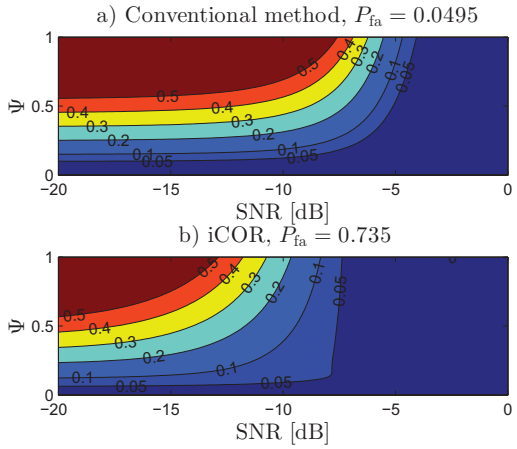

Fig. 4. Contour plot of RMSE vs SNR and Ψ, $M = 1000$, ideal ED with $N = 100$, a) conventional method, b) iCOR, $\lambda_{\rm W,RMSE} = 0.05$, Bernoulli model.

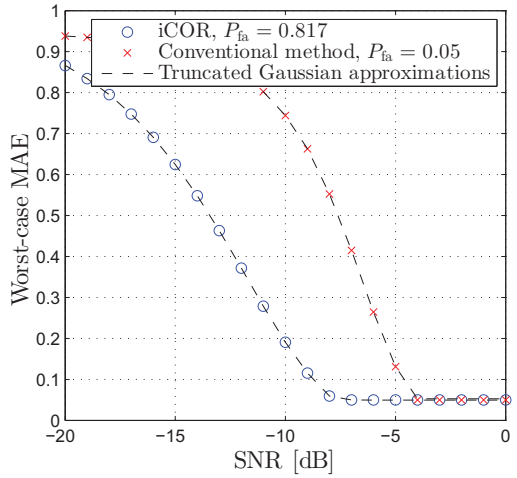

Fig. 5. Worst-case MAE, $M = 1000$, ideal ED with $N = 100$, $\lambda_{\rm W,MAE} = 0.05$, Bernoulli model.

$\lambda_{\rm W,RMSE} = 0.02$, the conventional method can use $P_{\rm fa} = 0.019$ while iCOR can use $P_{\rm fa} = 0.209$ (approximation (51) gives 0.29). Fig. 3 shows the worst-case RMSE as a function of $P_{\rm fa}$ for SNR $= -10$ dB. We can see that the optimal $P_{\rm fa}$ for the conventional method is around the point where $P_{\rm d} - P_{\rm fa}$ reaches its maximum. However, since the iCOR can suppress the effect of $P_{\rm fa}$, its optimal point is at $P_{\rm fa}$ of more than 0.9. Since the worst-case RMSE with $P_{\rm d} = 1$ is constrained, neither of these methods is able to use their optimal $P_{\rm fa}$ (for this particular SNR level). However, the iCOR can use $P_{\rm fa} = 0.735$, which is much closer to its optimal point than the conventional method tied to a very small value ($P_{\rm fa} = 0.0495$).

In Fig. 4, we show the RMSE contour as the functions of SNR and Ψ. The worst-case RMSE can be obtained by selecting for each SNR the highest value in the vertical direction corresponding to selecting the value of Ψ leading to the highest RMSE.

Fig. 5 shows the worst-case MAE for the iCOR and the conventional COR estimation methods for $M = 1000$ observations and ideal ED with $N = 100$ complex samples used for each observation. The constraint value used is $\lambda_{\rm W,MAE} = 0.05$. The gain of the proposed iCOR method is around 4–7 dB. By comparing Fig. 5 with the results for ideal ED in Fig. 1 we observe that the results for MAE and RMSE do not have significant differences.

C. Effect of the Signal Occupancy Model

In order to show the impact of the signal occupancy model, we use a smaller number of samples than above, since for large values of M the occupancy model is not significantly affecting the results. Fig. 6 shows the results for $M = 110$. The improvement of the iCOR estimate over the conventional method observed in Fig. 6 is less than 1 dB for the Bernoulli

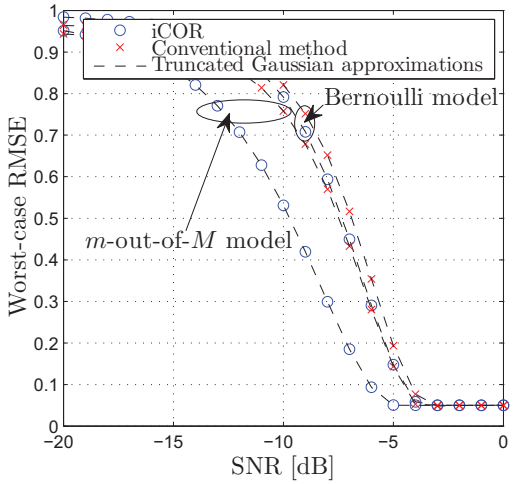

Fig. 6. Worst-case RMSE, $M = 110$, ideal ED with $N = 100$, $\lambda_{\mathrm{W,RMSE}} = 0.05$, Bernoulli and m-out-of-M models.

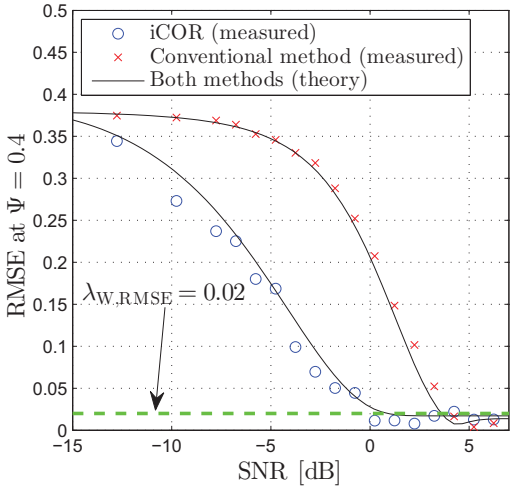

Fig. 7. Real measurement and theoretical results, AWGN channel (theory and measurement), 802.11b signal (measurement), Gaussian signal (theory), $\Psi = 0.4$, $\lambda_{\mathrm{W,RMSE}} = 0.02$ (shown with a green dashed line), $M = 5000$.

model, but it can be up to 4 dB, which is a remarkable improvement, under the m-out-of-M model. Thus, for the m-out-of-M model the iCOR significantly improves performance compared to the conventional method. The reason for this behaviour lies in the allowed P_{fa} values. The allowed P_{fa} for the conventional method is 0.0279 for the Bernoulli model and 0.0459 for the m-out-of-M model. For the iCOR solutions, the allowed P_{fa} is 0.047 for the Bernoulli model and 0.239 for the m-out-of-M model. The truncated Gaussian approximation still gives very good accuracy.

D. Experimental Results

The measurement results in Fig. 7 for the AWGN channel validate the iCOR method and also show an excellent fit between the experimental and theoretical results. Small differences result from the random signal model not being exact and from the limited number of measurement samples.

In Fig. 7, for SNR values around 5 dB, it is observed that the theoretical RMSE for the conventional method increases with the SNR and then converges to a final level. Usually, the RMSE is a non-increasing function of the SNR. This behavior is caused by the false alarms. When $P_{\mathrm{d}} = 1$, the false alarms can only be harmful. When P_{d} is close to one, the false alarms can offset the loss due missing actual signals.

The RMSE at high SNR can be smaller for the conventional method. The reason is the fact that we limit the worst-case RMSE to the worst actual COR level. The conventional method has its worst RMSE, when the actual COR is around zero, but the iCOR estimate has its worst RMSE at a higher COR level. The value $\Psi = 0.4$ utilized in the experiments is closer to the COR level leading to the worst-case RMSE for the iCOR than that for the conventional method.

Fig. 8 shows the results with the ETSI BRAN A WLAN channel model. For the theoretical results we use the Rayleigh fading channel model providing excellent fit to the measurements.

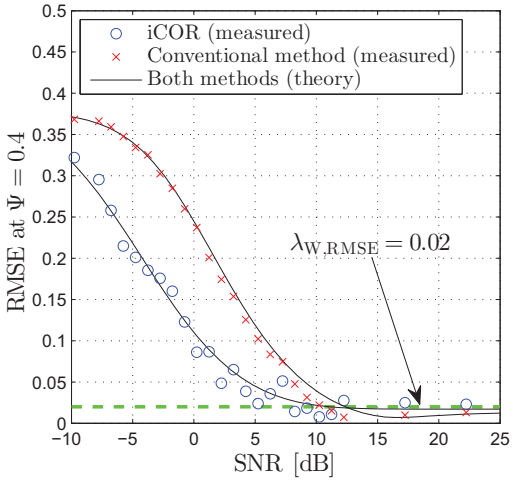

Fig. 8. Real measurement and theoretical results, ETSI BRAN-A WLAN channel (measurement), Rayleigh fading (theory), 802.11b signal (measurement), Gaussian signal (theory), $\Psi = 0.4$, $\lambda_{\mathrm{W,RMSE}} = 0.02$ (shown with a green dashed line), $M = 5000$.

VIII. Optimized Mapping Functions

We may ask: is the mapping function (48) for the proposed iCOR method optimal? We already know that it is the MLE for $P_{\mathrm{d}} = 1$. However, this does not imply the optimality for the RMSE. In this section, we compare the iCOR to two differently optimized mapping functions with the m-out-of-M model.

A. RMSE-optimal for $P_{\mathrm{d}} = 1$

We find the weights for $P_{\mathrm{d}} = 1$ that are optimal in terms of the worst-case RMSE when $P_{\mathrm{d}} = 1$. The optimization problem

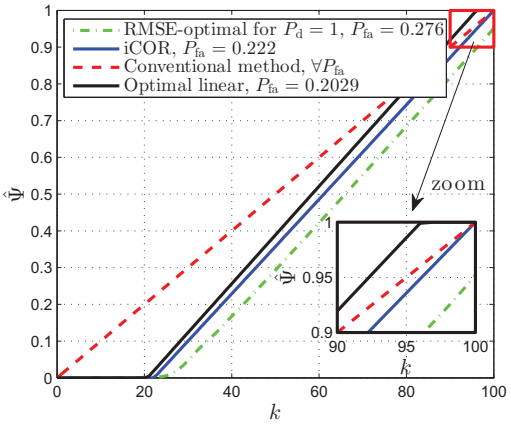

Fig. 9. Mapping function from k to $\hat{\Psi}$ for RMSE-optimal weights for $P_{\mathrm{d}} = 1$, iCOR, conventional method, and optimized linear weights, $M = 100$, ideal ED with $N = 100$, m-out-of-M model, $\lambda_{\mathrm{W,RMSE}} = 0.05$.

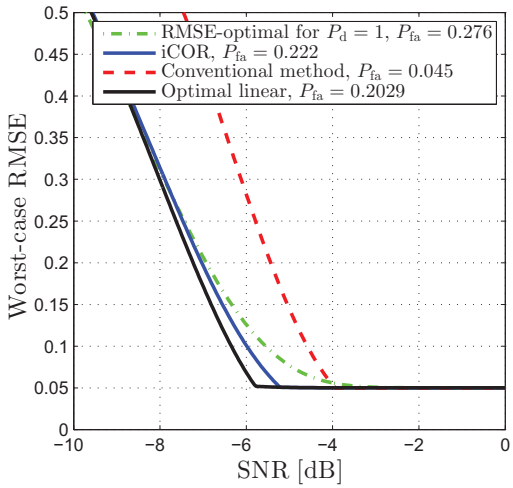

Fig. 10. Worst-case RMSE for RMSE-optimal weights for $P_{\mathrm{d}} = 1$, iCOR, conventional method, and optimized linear weights, ideal ED with $N = 100$, m-out-of-M model, $\lambda_{\mathrm{W,RMSE}} = 0.05$.

for a given P_{fa} is

$$\min_{\boldsymbol{\Xi}} \left[\max_{m\in\{0,1,\cdots,M\}} \left\{ \sum_{k\in\{0,1,\cdots,M\}} p_k \left(\xi_k - \frac{m}{M}\right)^2 \right\} \right], \quad (53)$$

where $\boldsymbol{\Xi} = [\xi_0\ \xi_1\ \cdots\ \xi_M]$ corresponds to an arbitrary vector mapping k to $\hat{\Psi}$ and p_k is found with (23) assuming $P_{\mathrm{d}} = 1$. We solve the optimization problem and increase the target P_{fa} value as long as the worst-case RMSE-optimal mapping function satisfies the $\lambda_{\mathrm{W,RMSE}}$ constraint. This leads to the mapping function allowing the highest possible P_{fa} for the specified constraint $\lambda_{\mathrm{W,RMSE}}$.

B. Optimized Linear

We numerically optimize the coefficients a_1 and a_0 of the linear function (30). The optimization target was to find the coefficients that minimize the required SNR for reaching the worst-case RMSE of 0.1 (corresponding to $2\lambda_{\mathrm{W,RMSE}}$) while satisfying the constraint $\lambda_{\mathrm{W,RMSE}}$. The aim here is to not only optimize for $P_{\mathrm{d}} = 1$ but also to consider weaker signals for which $P_{\mathrm{d}} < 1$.

C. Results for Mapping Function and Worst-case RMSE

For $M = 100$ and $\lambda_{\mathrm{W,RMSE}} = 0.05$, the resulting mapping functions are presented in Fig. 9. The RMSE-optimal weights for $P_{\mathrm{d}} = 1$ are slightly non-linear and allow using the highest P_{fa} from all the considered methods as it should be, because this was the optimization target. However, as shown in Fig. 10, even with the higher P_{fa}, the performance of the RMSE-optimal mapping function for $P_{\mathrm{d}} = 1$ is worse for medium signal power levels than the performance of the iCOR method. This is because the mapping function optimized for $P_{\mathrm{d}} = 1$ is not necessarily optimal for lower SNR values. The RMSE-optimal mapping function for $P_{\mathrm{d}} = 1$ uses $\hat{\Psi}$ less than 1 even when $k = M$. When the signal power is reduced, signals are not always detected, i.e., $P_{\mathrm{d}} < 1$. In this case, it would be better to use higher output COR values to compensate for the undetected signals. In fact, the optimized linear mapping function is doing exactly this. It has the highest output COR from all the considered methods for large values of k. The iCOR was also found assuming $P_{\mathrm{d}} = 1$ (it is MLE for $P_{\mathrm{d}} = 1$). However, its output is significantly larger at high values of k than the RMSE-optimal mapping function for $P_{\mathrm{d}} = 1$, leading to better performance when $P_{\mathrm{d}} < 1$. The conventional method also has large output values at high values of k, but it greatly suffers from too large output when k is small (leading to no suppression of false alarms). The linear mapping function has a slightly better performance than iCOR. However, the performance of the iCOR is close and a significant amount of computation is required to find the optimal linear mapping function. Thus, the iCOR presents an excellent compromise between the complexity and performance.

IX. Conclusion

The objective of this work was to consider estimation of the channel occupancy rate. The proposed iCOR method is able to suppress the effect of false alarms unlike the conventional COR estimation method. Comprehensive theoretical analysis was performed. The numerical and experimental results confirm that the iCOR significantly outperforms the conventional method. Thus, the iCOR method can be applied for more accurate COR estimation than possible with the conventional method for both spectrum utilization measurement campaigns and spectrum utilization measurements during operation of a cognitive transmitter. In the future work, methods with knowledge of the SNR will be considered for obtaining a higher performance but requiring more information. We will also consider other noise uncertainty models in addition to the ENP-ED such as the bounded worse behaviour (BWB) model [7]. Other interesting topics for future research include considering actual operation of secondary users with their spectrum sensing being assisted with COR measurements for assessing the secondary user communication rates.

APPENDIX A

Proof that the maximum allowed P_{fa} for conventional COR estimation under Bernoulli model is (42)*:* The RMSE is given in (39). For $P_{\mathrm{d}} = 1$ and given P_{fa}, the extremum point obtained by solving $\frac{d[\mathrm{mse}(\Psi)]}{d\Psi} = 0$ (extremum points are the same for mse and rmse) is

$$\Psi\left(P_{\mathrm{fa}}\right) = \frac{3P_{\mathrm{fa}} + 2MP_{\mathrm{fa}}^2 - 2P_{\mathrm{fa}}^2 - 1}{4P_{\mathrm{fa}} + 2MP_{\mathrm{fa}}^2 - 2P_{\mathrm{fa}}^2 - 2} \tag{54}$$

which is valid, i.e., $\Psi \in [0\ 1]$, if

$$0 \leq P_{\mathrm{fa}} \leq \frac{\sqrt{8M+1} - 3}{4\left(M-1\right)} \tag{55}$$

The MSE for the extremum point is

$$-\frac{\left(P_{\mathrm{fa}} - 1\right)^2}{4M\left(2P_{\mathrm{fa}} + MP_{\mathrm{fa}}^2 - P_{\mathrm{fa}}^2 - 1\right)} \tag{56}$$

The MSE for the boundary point $\Psi = 0$ is

$$\frac{P_{\mathrm{fa}}}{M} + P_{\mathrm{fa}}^2\left(1 - \frac{1}{M}\right) \tag{57}$$

As the extremum point MSE is always greater than or equal to MSE of $\Psi = 0$ (within its validity region), we get that the worst-case MSE is

$$\begin{cases} -\frac{\left(P_{\mathrm{fa}}-1\right)^2}{4M\left(2P_{\mathrm{fa}}+MP_{\mathrm{fa}}^2-P_{\mathrm{fa}}^2-1\right)} & 0 \leq P_{\mathrm{fa}} \leq \frac{\sqrt{8M+1}-3}{4(M-1)} \\ \frac{P_{\mathrm{fa}}}{M} + P_{\mathrm{fa}}^2 - \frac{P_{\mathrm{fa}}^2}{M} & \text{otherwise} \end{cases} \tag{58}$$

This results into maximum allowed P_{fa} given by (42). ■

REFERENCES

[1] "Expanding America's leadership in wireless innovation," The White House, Washington D.C., Jun. 2013.

[2] Q. Zhao and B. M. Sadler, "A survey of dynamic spectrum access," *IEEE Signal Process. Mag.*, vol. 24, no. 3, pp. 79–89, May 2007.

[3] Federal Communications Commission, "Second memorandum opinion and order, FCC 10-174," Sep. 2010.

[4] I. F. Akyildiz, W.-Y. Lee, M. C. Vuran, and S. Mohanty, "A survey on spectrum management in cognitive radio networks," *IEEE Commun. Mag.*, vol. 46, no. 4, pp. 40–48, Apr. 2008.

[5] T. Yücek and H. Arslan, "A survey of spectrum sensing algorithms for cognitive radio applications," *IEEE Commun. Surveys Tuts.*, vol. 11, no. 1, pp. 116–130, 2009.

[6] M. López-Benítez and F. Casadevall, "Signal uncertainty in spectrum sensing for cognitive radio," *IEEE Trans. Commun.*, vol. 61, no. 4, pp. 1231–1241, Apr. 2013.

[7] A. Mariani, A. Giorgetti, and M. Chiani, "Effects of noise power estimation on energy detection for cognitive radio applications," *IEEE Trans. Commun.*, vol. 59, no. 12, pp. 3410–3420, Dec. 2011.

[8] Y. Zeng, Y.-C. Liang, A. T. Hoang, and R. Zhang, "A review on spectrum sensing for cognitive radio: Challenges and solutions," *EURASIP J. Adv. Signal Process*, vol. 2010, Jan. 2010.

[9] M. Wellens, A. Baynast, and P. Mähönen, "On the performance of dynamic spectrum access based on spectrum occupancy statistics," *IET Commun.*, vol. 2, no. 6, pp. 772–782, Jul. 2008.

[10] K. Umebayashi, Y. Suzuki, and J. Lehtomäki, "Dynamic selection of CWmin in cognitive radio networks for protecting IEEE 802.11 primary users," in *Proc. CROWNCOM*, Jun. 2011, pp. 266–270.

[11] "1000x: More spectrum-especially for small cells," Tech. Rep., Nov. 2013. [Online]. Available: http://www.qualcomm.com/media/documents/files/1000x-more-spectrum-especially-for-small-cells.pdf

[12] K. Chintalapudi, B. Radunovic, V. Balan, M. Buettener, S. Yerramalli, V. Navda, and R. Ramjee, "WiFi-NC: WiFi over narrow channels," in *Proc. NSDI*, 2012.

[13] M. López-Benítez and F. Casadevall, "Methodological aspects of spectrum occupancy evaluation in the context of cognitive radio," *European Trans. Telecommun.*, vol. 21, no. 8, pp. 680–693, Dec. 2010.

[14] A. D. Spaulding and G. H. Hagn, "On the definition and estimation of spectrum occupancy," *IEEE Trans. Electromagn. Compat.*, vol. 19, no. 3, pp. 269–280, Aug. 1977.

[15] R. Bacchus, T. Taher, K. Zdunek, and D. Roberson, "Spectrum utilization study in support of dynamic spectrum access for public safety," in *Proc. DySPAN*, Apr. 2010.

[16] J. Lehtomäki, R. Vuohtoniemi, and K. Umebayashi, "On the measurement of duty cycle and channel occupancy rate," *IEEE J. Sel. Areas Commun.*, vol. 31, no. 11, pp. 2555–2565, Nov. 2013.

[17] M. Biggs, A. Henley, and T. Clarkson, "Occupancy analysis of the 2.4 GHz ISM band," *IEE Proc. Commun.*, vol. 151, no. 5, pp. 481–488, Oct. 2004.

[18] M. Wellens and P. Mähönen, "Lessons learned from an extensive spectrum occupancy measurement campaign and a stochastic duty cycle model," *Mobile Netw. Appl.*, vol. 15, no. 3, pp. 461–474, 2010.

[19] M. Wellens, J. Riihijärvi, and P. Mähönen, "Empirical time and frequency domain models of spectrum use," *Phys. Commun.*, vol. 2, no. 1-2, pp. 10–32, Mar. 2009.

[20] M. López-Benítez and F. Casadevall, "Time-dimension models of spectrum usage for the analysis, design, and simulation of cognitive radio networks," *IEEE Trans. Veh. Technol.*, vol. 62, no. 5, pp. 2091–2104, Jun. 2013.

[21] S. Wang, F. Patenaude, and R. J. Inkol, "Computation of the normalized detection threshold for the FFT filter bank-based summation CFAR detector," *Journal of Computers*, vol. 2, no. 6, pp. 35–48, Aug. 2007.

[22] J. Naganawa, H. Kim, S. Saruwatari, H. Onaga, and H. Morikawa, "Distributed spectrum sensing utilizing heterogeneous wireless devices and measurement equipment," in *Proc. DySPAN*, May 2011, pp. 173–184.

[23] J. J. Lehtomäki, R. Vuohtoniemi, K. Umebayashi, and J.-P. Mäkelä, "Energy detection based estimation of channel occupancy rate with adaptive noise estimation," *IEICE Trans. Commun.*, vol. E95-B, no. 4, pp. 1076–1084, Apr. 2012.

[24] K. Umebayashi, R. Takagi, N. Ioroi, J. Lehtomäki, and Y. Suzuki, "Duty cycle and noise floor estimation with Welch FFT for spectrum usage measurements," in *Proc. CROWNCOM*, Oulu, Finland, Jun. 2014.

[25] M. Abramowitz and I. Stegun, *Handbook of Mathematical Functions*. New York: Dover, 1964.

[26] J. J. Lehtomäki, M. Juntti, and H. Saarnisaari, "CFAR strategies for channelized radiometer," *IEEE Signal Process. Lett.*, vol. 12, no. 1, pp. 13–16, Jan. 2005.

[27] F. J. Harris, "On the use of windows for harmonic analysis with the discrete Fourier transform," *Proc. IEEE*, vol. 66, no. 1, pp. 51–83, 1978.

[28] J. P. Imhof, "Computing the distribution of quadratic forms in normal variables," *Biometrika*, vol. 48, no. 3/4, pp. 419–426, Dec. 1961.

[29] N. Johnson, S. Kotz, and N. Balakrishnan, *Continuous univariate distributions*. Wiley, 1994, vol. 1.

[30] F. Leone, R. Nottingham, and L. Nelson, "The folded normal distribution," *Technometrics*, vol. 3, no. 4, pp. 543–550, 1961.